Self-Built Tensile Strain in Large Single-Walled Carbon Nanotubes

Pingqi Gao,[†,‡] Lianxi Zheng,[§] Qing Zhang,[‡,*] Shaoning Yuan,[‡] Yumeng You,[||] Zexiang Shen,[||] and Deyan He[†]

[†]Department of Physics, Lanzhou University, Lanzhou 730000, People's Republic of China, [‡]Microelectronics Center, School of Electrical and Electronic Engineering, Nanyang Technological University, S1-B2c-20, Singapore 639798, [§]School of Mechanical and Aerospace Engineering, Nanyang Technological University, Singapore 639798, and [||]Division of Physics and Applied Physics, School of Physical and Mathematical Sciences, Nanyang Technological University, 21 Nanyang link, Singapore 637371

ABSTRACT Abnormal Raman scattering from a large-diameter ultralong single-walled carbon nanotube (SWCNT) is studied in detail. Along the SWCNT, the Raman spectra show the frequencies of 1553, 1563, and 2597 cm^{-1} for G$^+$, G$^-$, and G' peaks, respectively, much lower than the corresponding frequencies well-reported both experimentally and theoretically. The significant downshifts in the peaks frequencies can be attributed to self-built tensile strain, which is likely caused by carbon nanodots decorated on the tube. After infrared laser heating is performed to one point of it, all of the Raman modes are found to shift to higher frequencies and approach their conventional values. We suggest that the SWCNTs with larger diameters easily possess such self-built strain compared to small-diameter SWCNTs because of the weaker curvature effect for the larger ones.

KEYWORDS: carbon nanotube · Raman · strain · deformation · microscopy

Studying the impact of mechanical deformations on the electronic structures and electronic transport properties of single-walled carbon nanotubes (SWCNTs) is of both fundamental and application interests. Several experimental observations have confirmed that the band gap of the SWCNTs can be altered significantly by the strain.[1,2] The magnitude of the band gap change under uniaxial strain is found to be about 80 meV per 1% strain, in good agreement with theoretical predictions.[3] This opens an opportunity of engineering the band gap of the SWCNTs through introducing a controllable strain. In order to fully embrace such an opportunity, the mechanism of structure deformation under different strains must be studied first.

Resonance Raman spectroscopy is widely used to characterize the structure deformation of the individual SWCNTs because of its strength on studying the structural properties under various external perturbations, including electrostatic gating, electrochemical gating, temperature and strain, etc.[4−6] For example, the deformation of carbon fibers as a function of the applied strain has been studied using in situ Raman spectroscopy.[7,8] It has been reported that the tangential Raman modes (G band) of the SWCNTs shift to lower wavenumbers under a uniaxial tensile strain. A moderate strain can adjust the Van Hove singularities of SWCNTs, which can be seen from the Raman intensity changes.[9] Cronin et al.[10,11] have observed that the in-plane vibration frequencies are lowered by as much as 1.5% (40 cm^{-1} for G' band), while the radial breathing mode (RBM) remains unchanged for tensile strains from 0.06 to 1.65%. Duan et al. have found that torsional strain can induce a large downshift in the E_2 symmetry mode in the G$^+$ band but slight upshift for the rest of the G mode and the RBM mode.[12] All of those experimental results indicate that Raman spectroscopy is a powerful tool for identifying any small structural change and capable for quantitative study of the strain in the SWCNTs.

In this study, abnormal Raman scattering, indicated by the Raman spectrum frequencies of 1553, 1563, and 2597 cm^{-1} for G$^-$, G$^+$, and G' peaks, respectively, has been observed from a semiconducting large-diameter (~1.9 nm) and ultralong (~1 mm) SWCNT. These Raman frequencies are much lower than the corresponding frequencies well-reported both experimentally and theoretically. The Raman features remain identical along the whole SWCNT. However, the peaks shift back to higher frequencies and approach their normal values after the SWCNT is heated by an infrared laser. The big downshifts in the Raman frequencies and the subsequent recovery caused by the heating can be attributed to the self-built tensile strain induced by
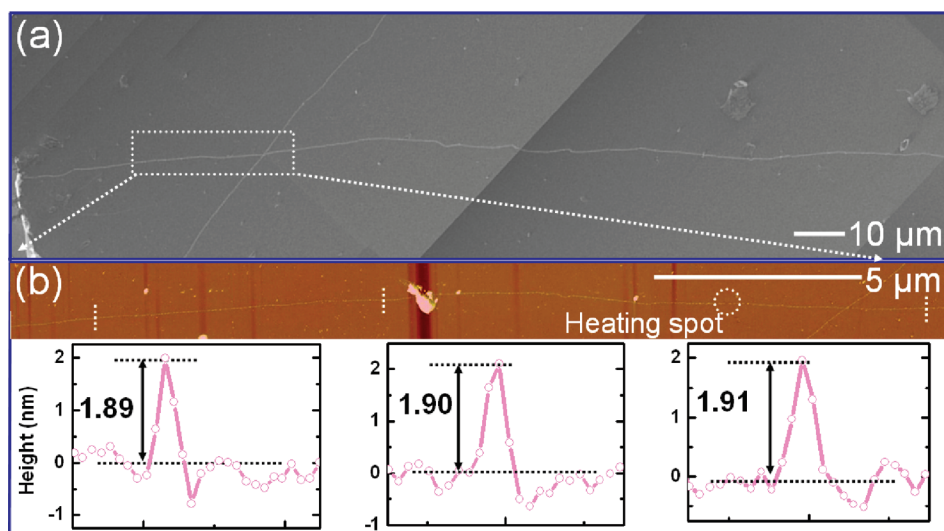
Figure 1. (a) Typical SEM image of a large-diameter and ultralong SWCNT that is used in this study. The total length is more than 0.1 cm, and only the initial part of 250 μm long is shown here. (b) AFM image of the section in the rectangle area shown in (a). Three AFM height profiles were obtained at the three dashed lines. The dashed circle marks the 785 nm laser heating spot.

decorated carbon nanodots and the laser-heating-induced strain relaxation, respectively.

RESULTS AND DISCUSSION

The SWCNTs used in this work were synthesized by ethanol chemical vapor deposition on Si/SiO$_2$ substrates.[13] The tubes are found to be well-separated from each other. Most of the SWCNTs are longer than 100 μm, and many extend in length up to a centimeter.[14] Figure 1a is a scanning electron microscopy (SEM) image of such SWCNTs, showing one straight SWCNT starting from the left edge of the substrate. The atomic force microscopy (AFM) image of this SWCNT and its height profiles are shown in Figure 1b. From the AFM height profiles measured at different locations (indicated by dashed lines shown in the AFM image), one can find that the tube diameter is around 1.9 nm. (Note that the diameters are measured in the locations where there are no carbon nanodots; see Figure 3.) A series of Raman scatterings along this tube, with a step of 10 μm from the left to the right, have been performed. All of the measured Raman spectra are identical to the one shown in Figure 2a. The enlarged RBM, G, and G′ bands are shown in Figure 2b−d, respectively. The RBM peak is centered at $\omega_{RBM} = 132$ cm^{-1} with a narrow line width of 5 cm^{-1}, from which the tube diameter can be calculated as $d_t \sim 1.88$ nm using the relation of $d_t = 248/\omega_{RBM}$.[15] This value is consistent with our AFM observations. The G band shows two peaks, with ω_{G^+} at 1563 cm^{-1} and ω_{G^-} at 1553 cm^{-1}. Their shapes suggest that this SWCNT is a semiconducting tube.[16] The G′ band can also be divided into two peaks located at 2597 and 2664 cm^{-1}. The 2664 cm^{-1} peak can be attributed to the amorphous carbon coated on the substrate surface during the SWCNT growth, which can also

be observed in the area (of the same substrate) where there is no SWCNT.

To understand our Raman observations, we first calculate the theoretical values of ω_{G^+}, ω_{G^-}, and $\omega_{G'}$ for a 1.88 nm semiconducting SWCNT. Since the value of 1591 cm^{-1} for ω_{G^+} is widely accepted and is insensitive to the tube diameter, we can calculate ω_{G^-}, and $\omega_{G'}$ using the expression $\omega = \omega_0 + \beta/d^n$, where ω_0, β, and n are the frequency of two-dimensional (2-D) graphite, the coefficient, and the exponent of the diameter de-
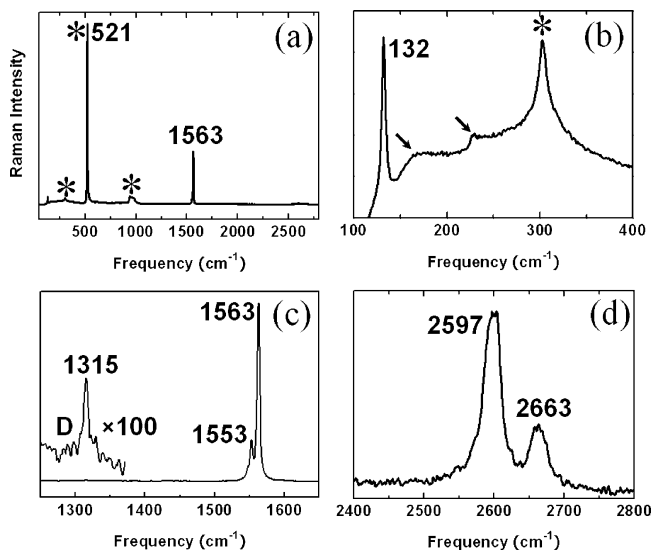

Figure 2. (a) Full Raman spectra of the SWCNT (horizontal one in Figure 1). (b−d) Expanded spectra of RBM, G, and G′ modes, respectively. In addition, the D band is also shown in panel c with 100 times enlargement in intensity. Note that the Raman spectra were measured along the tube axis with a step of 10 μm from the left to right, up to 0.1 cm in total. All of the spectra acquired are identical. Peak positions are labeled. The isolated nanotube is sitting on a SiO$_2$/Si substrate whose Raman peaks are denoted by ∗ and are used for the calibration purpose. The two kinks in panel b indicated by the arrows are caused by the Raman system.
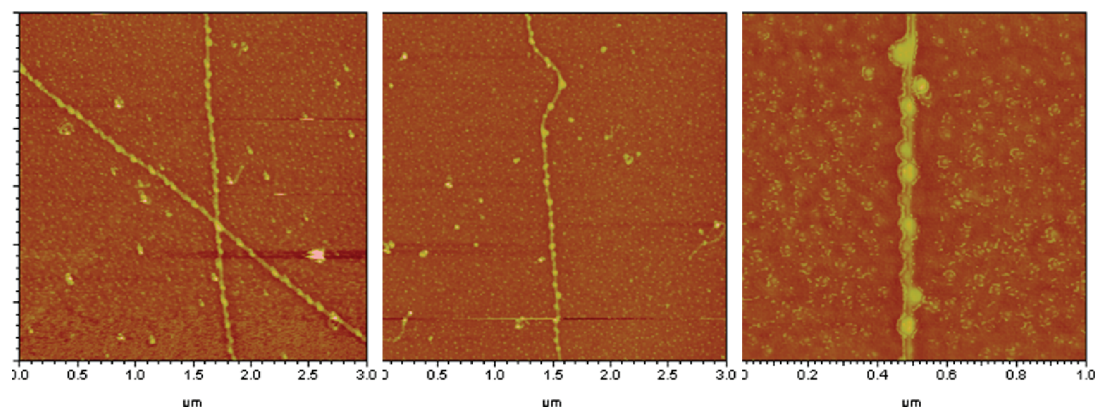
Figure 3. High-resolution AFM images of different locations of the same SWCNT shown in Figure 1.

pendence, respectively.[16,17] With the ω_0, β, and n of 1591 cm^{-1}, -45.7 cm^{-1}*nm (for semiconducting SWCNTs), and 2, respectively, the theoretical value of ω_{G^-} for a 1.88 nm SWCNT should be 1578 cm^{-1}.[16] Similar for the double resonance G′ mode, we have $\omega_0 = 2708.1$ cm^{-1} (for excited photon energy $E_L = 2.41$ eV), $\beta = -35.4$ cm^{-1}*nm, and $n = 1$.[16] Because the dependences of the $\omega_{G'}$ on d_t and excited photon energy (E_L) must be considered, we use the dispersive relation of $\omega_{G'}$ with E_L as $\Delta\omega_{G'} = 90$ cm^{-1} eV^{-1}.[18] Then the theoretical G′ frequency under the 1.96 eV laser (the laser line used in this study) conditions can be calculated as $\sim$2650 cm^{-1}. These calculated values are also confirmed in experimental measurements.[17,19] Comparing these values with our Raman measurements, one can easily find that ω_{G^-}, ω_{G^+}, and $\omega_{G'}$ for our SWCNT are downshifted by a large quantity of 25, 28, and 53 cm^{-1}, respectively.

Possible reasons for such big downshifts in phonon frequencies include the variations in temperature, charge density, chemisorption and strain, *etc*. Since all of the Raman measurements were carried out at room temperature and no broad line width has been observed, we can safely exclude the temperature effect. In addition, a charge of $\sim$6 $\times$ 10^6 e cm^{-1} (where e is the unit charge of 1.6 $\times$ 10^{-19} C) could account for the 5 cm^{-1} shift of the G band according to the results of gate-voltage-tuned Raman spectroscopy of SWCNTs.[20] Thus, even if we assume that the variation of the charge carrier density from the substrate or chemical absorbants to the SWCNT is at the level of 8 $\times$ 10^6 e cm^{-1} (the saturated charge of the tube itself), the shift in G band frequency should be less than 7 cm^{-1}, much smaller than our observed shift of $\sim$28 cm^{-1}.[21] Therefore, charge effect should not be the dominate origin of the significant downshifts. Recent experiments reported that hydrogen chemisorption onto SWCNTs can result in the carbon–carbon bond (C–C) expand in both axial and radial directions.[22,23] Such a hydrogenation process only can occur at the condition of high energy treatments in order to break sp^2 C–C and form sp^3 C–H, which always induces a relative strong D

band. However, as shown in Figure 2c, the D band is still very weak even after 100 times enlargement in intensity. Thus, self-built strain seems to be responsible for the large downshifts. A tensile strain can elongate the C–C bonds and weaken their energy and, therefore, lower the vibrational frequency.

How could the strain be built up in our SWCNT? Two possibilities: substrate-induced tensile strain and/or self-built tensile strain. If thermal contraction is different for SWCNTs and Si/SiO$_2$ upon cooling after the growth process, the SWCNTs should, in fact, be expected to be under strain stress. However, the coefficient of the thermal expansion calculated for SWCNTs is very close to that of Si/SiO$_2$.[24] Another concern is that, as the substrate is not smooth due to the existence of defects and steps and the cooling rate is not uniform, the strain induced by the SiO$_2$ substrate (if any) should be localized spatially. These are not in agreement with our observation where the tensile strain is uniform at a large distance in the SWCNT. Thus substrate-induced tensile strain is not the key factor.

The distinctly abnormal Raman spectrum implies that the structure of the tube we studied should have some differences to normal cases. Figure 3 shows the AFM images collected from different parts of the same tube. A structure of SWCNT with nanodots can be clearly seen (similar structures have been found for all tubes we studied). The tube may serve as a template for the ordering and orientation of the nanodots along the nanotube axis. The nanodots are decorated on the tube with an average height of 5 nm and an average distance of 90 nm between them. These nanodots may form from accumulation of carbon species from ethanol CVD during the synthesis process. Compared to a pristine SWCNT, the decorated carbon nanodots could cause structural disturbance and physical strain in the tube, leading to the significant downshifts. Similar to the strain induced by AFM tip, the strains caused by the carbon nanodots are also not confined to a small region where the tube is distorted, but rather extend for long distances along the length of the SWCNT.
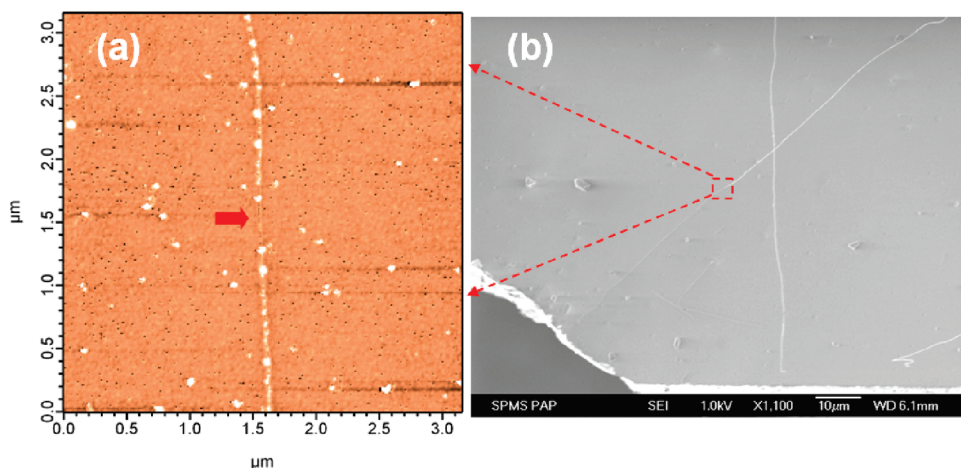
Figure 4. (a) High-resolution AFM image near the laser heating point. The red arrow indicates the burnt-off spot. (b) SEM image after the laser heating.

The existence of the tensile strain is supported by the following laser-induced strain−relaxation process. A beam of 785 nm laser (with a power of 15 mW and a beam diameter of 600 nm through a $100\times$ air objective) has been introduced to heat the SWCNT at the location circled in Figure 1b for 10 min. After the heating, we viewed the SWCNT at the location using SEM and AFM (see Figure 4). The AFM image shows that the tube has been burnt off with a gap of 1 μm. Compared to Figure 1a, the SEM image of Figure 4b shows apparently different contrasts of the tube beside the burnt-off point, suggesting the different charging effects on the two parts of it.

Figure 5a−d shows the RBM, G, D, and G′ band frequency changes as functions of the position along the tube after the laser heating. The detailed Raman spectra for each band are also shown in Figure 5e−h. For simplicity, we set the burnt-off point as $x = 0$ and divided the tube into three regions; that is, Region I (from $x = -25$ to 30 μm) is the area that was directly heated by the laser beam, while Region II (left) and Region III (right) are the regions on the two sides of Region I. After the laser heating, all of the Raman modes were been found to shift to high frequencies, approaching their theoretical values. The recovery in Region I is more significant than Regions II and III (see Figure 5a−d). The maximum upshifts occur at the position of $x = 0$, and they are 8, 20, 23, 22.5, and 46 cm^{-1} for the RBM, G$^-$, G$^+$, D, and G′, respectively. In Regions III (II), such upshifts are slightly moderate, at 2 (5.5), 13 (13.5), 18 (18.5), 17.5 (18.5), and 36 (39) cm^{-1}, respectively, for the corresponding Raman peaks. The G′ mode, as an overtone of the first-order

D band, is not exactly twice ω_D (1315 cm^{-1}). However, it shows a roughly twice as large shift when compared to the D band. Although the upshifts in Region II are slightly different from Region III, such upshifts are almost identical within each region (II or III). One can find, from Figure 5f, that the 2664 cm^{-1} peak from amorphous carbon does not show a significant difference before and after the heating, sug-
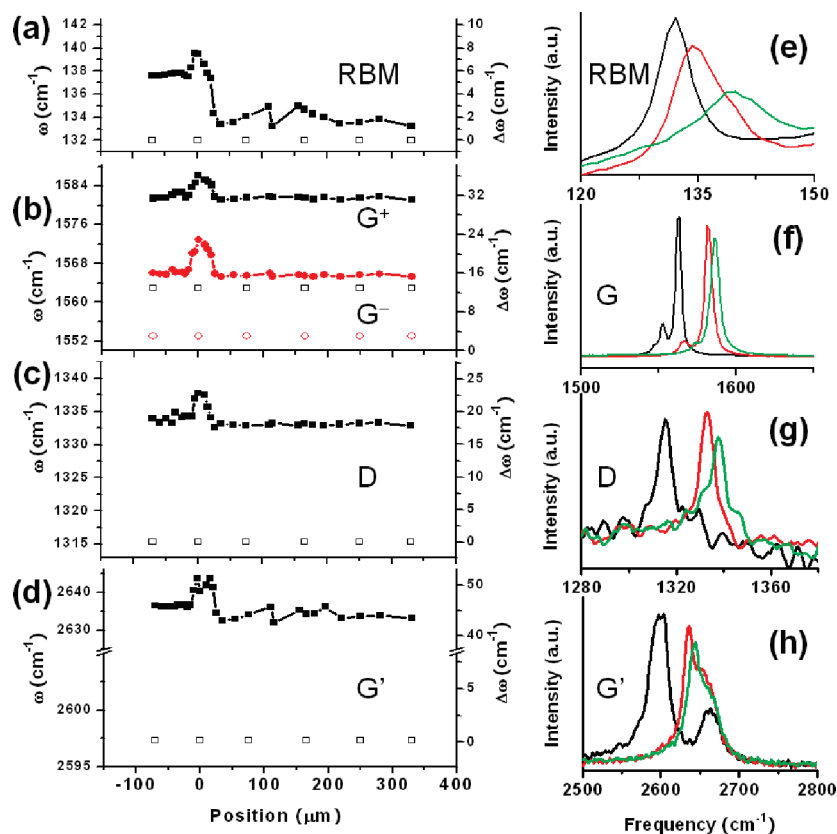

Figure 5. (a−d) Profiles of ω_{RBM}, ω_G, ω_D, and $\omega_{G'}$ vs the position along the tube shown in Figure 1. Open and filled squares (dots) are the frequencies before and after the laser heating. Red dots and black squares in panel b denote the frequencies of G$^-$ and G$^+$, respectively. (e−h) Raman spectra of RBM, G, D, and G′ modes, respectively. The black line is the spectra before the heating, while red and green lines are spectra after the heating from Region III and $x = 0$, respectively.

TABLE 1. Frequencies of the Raman Modes of Six Different SWCNTs on the Same Substrate[a]

ω_{RBM} [cm^{-1}]	d_t [nm]	ω_{G^-} [cm^{-1}]	ω_{G^+} [cm^{-1}]	$\omega_{G'}$ [cm^{-1}]
174	1.43	1560	1591	2648
162	1.53	1569	1590	2654
159	1.56	1572	1596	2658
132 (138)	1.88 (1.80)	1553 (1573)	1563 (1586)	2597 (2643)
135 (140)	1.84 (1.77)	1555 (1567)	1567 (1582)	2617 (2644)
124 (125.5)	2.00 (1.98)	1568 (1578)	1577 (1590)	2613 (2649)

[a]The listed values are the original frequencies before laser heating. For some unusual peaks, the maximum frequencies after heating are also listed in the parentheses. The diameters are determined from the equation $d_t = 248/\omega_{RBM}$.[14]

gesting that the laser heating does not affect amorphous carbon. More interestingly, from Figure 5a,d, one can see that the RBM mode demonstrates behavior simiar to that of D, G, and G' bands, showing up to 8 cm^{-1} upshift in frequency. This finding is totally different from previous studies on AFM tip-induced strains by other groups, in which no observable shift in RBM frequency was observed even when a uniaxial strain of 1.65% was applied.[10,12] Theoretical results also suggest that the radii of the nanotubes do not change under a substantially large uniaxial strain, even the C−C bond length varies up to 6%.[22] This is because the bonds along the circumference, partly strengthened by curvature effects, are not significantly affected by uniaxial strains orthogonal to them. The upshift in RBM frequency in Regions II and III can be tentatively attributed to the recovery from possible axial deformations caused by the carbon nanodots, while further upshift in Region I might reflect the fact that the tube is thinner and even burnt off. The G band phonons typically result from the motion of the carbon atoms tangential to the surface of the nanotube. The two components of this band for semiconducting SWCNTs correspond to the vibrations along the nanotube axis G$^+$ and in the circumferential direction G$^-$, respectively.[23] From the depression and subsequent recovery in ω_{G^-}, ω_{G^+}, we suggest that the C−C vibration along both directions could be affected by the initial strains.

The relaxation profile in Region I can be easily understood because it covered the whole broken part, where the most strain was released due to the elasticity of the deformations. Generally, the strain relaxation in one spot would cause a larger strain in other parts of the tube if it cannot move freely. However, in our case, even though the van der Waals bonding between the SWCNT and SiO$_2$ layer is strong, the strain relaxation is not confined in Region I but rather extends to the whole length of the tube in a very large distance (the range of our measurement was up to 300 μm). The observed strain relaxation is very uniform in Regions II and III. This is reasonable as the tensile strain could be released when the tem-

perature along the tube exceeds a critical value because of the high thermal conductivity of SWCNTs. The higher the local temperature, the more relaxation will result. The asymmetry of the frequency relaxation in Region II with respect to Region III could be attributed to a smaller heat dissipation in Region II than in Region III as the tube length in the two regions are different (70 μm for Region II and 1000 μm for Region III). The frequencies of the relaxed Raman modes are still slightly smaller than the theoretical values, especially for Regions II and III, implying that the relaxation is not fully completed and a small residue of strain still remains in the SWCNT.

One way to quantify the initial strain is the formula for the Grüneisen parameter $\gamma_{\omega_{G^+}}$ of the G$^+$ mode:

$$\gamma_{\omega_{G^+}} = -\frac{1}{\omega_{G^+}^0}\frac{\partial\omega_{G^+}}{\partial\varepsilon}$$

where $\omega_{G^+}^0$ is the G$^+$ peak position at zero strain; ε represents the longitudinal strain.[25] The parameter $\gamma_{\omega_{G^+}}$ has been successfully determined as 1.8 in graphene and 2.3 in the (8,0) SWNT, thus we can have $\gamma_{\omega_{G^+}} = 2$ for our 1.9 nm SWNT.[26,27] Then, the strain can be calculated as

$$\Delta\varepsilon = -\frac{1}{\omega_{G^+}^0}\frac{\Delta\omega_{G^+}}{\gamma_{\omega_{G^+}}} = -\frac{-28}{1591 \times 2} = 0.9\%$$

Cronin *et al.* reported a shift of the G$^+$ of 14.8 cm^{-1} for a strain of 0.53% in their SWNCTs, which is actually in reasonable agreement with our results.[10]

Statistically, we have carried out the Raman scattering from more than 40 different individual SWCNTs on the same substrate. Only six SWCNTs show clear RBM peaks due to the sharp resonance window. The peak positions of these SWCNTs are summarized in Table 1. For the three small-diameter SWCNTs, the G bands are normal and all of the frequencies of different Raman bands are consistent with the well-reported theoretical and experimental results. However, the large-diameter SWCNTs in Table 1 show large downshifts in the Raman frequencies. Similar laser heating process did cause upshifts in the frequencies (listed in parentheses of Table 1). However, the amount of the strain-induced frequency shifts and their recoveries vary from tube to tube, probably due to the chirality dependence of the strain.

Further experimental and simulation studies are needed to clarify the relation between the existence of carbon nanodots and the induced strain in SWCNTs. Another important evidence to support our viewpoint is that we did not find similar strain in bundled SWCNTs. This finding makes sense to us because the strain acted on each single tube in the bundle can be mitigated by its neighboring tubes. Figure 6a shows the SEM image of a tube with RBM peak at 135 cm^{-1}. This tube grows from the left to right and extends more than 1 cm. The Raman spec-

tra from different locations along the tube are quite different, as shown in Figure 6b−e. From Point 1 to Point 6, the Raman spectra are different from each other, while all spectra are identical after Point 6. Only one strong RBM peak at 135 cm^{-1} ($d_t \sim 1.84$ nm) is observed at Points 1 and 2. From Points 3 to 6, in addition to the 135 cm^{-1} peak, three other peaks at 163, 216, and 353 cm^{-1} are also clearly observed. This implies the tube has evolved from an individual 1.84 nm SWCNT at Points 1 and 2 to a small bundle containing several smaller-diameter SWCNTs after Point 3. The G band at the single tube part (Points 1 and 2) shows a strong peak at 1567 cm^{-1} and gradually changes to 1591 cm^{-1} when measuring it along the length toward Point 3. Similar evolutions can also be observed in the G′ peak (Figure 6d,e). This finding indicates that formation of a bundle can indeed prevent from the generation of strains.

CONCLUSION

Significant downshifts in the Raman spectra from large-diameter semiconducting SWCNTs have been observed. The Raman frequencies for the G$^-$, G$^+$, and G′ are 1553, 1563, and 2597 cm^{-1}, respectively, much lower than their theoretical and reported values. The Raman peaks can shift to higher frequencies and approach those normal values after the SWCNT is heated by an infrared laser beam. The big downshift in the Raman peak frequencies can be interpreted through a self-built tensile strain which
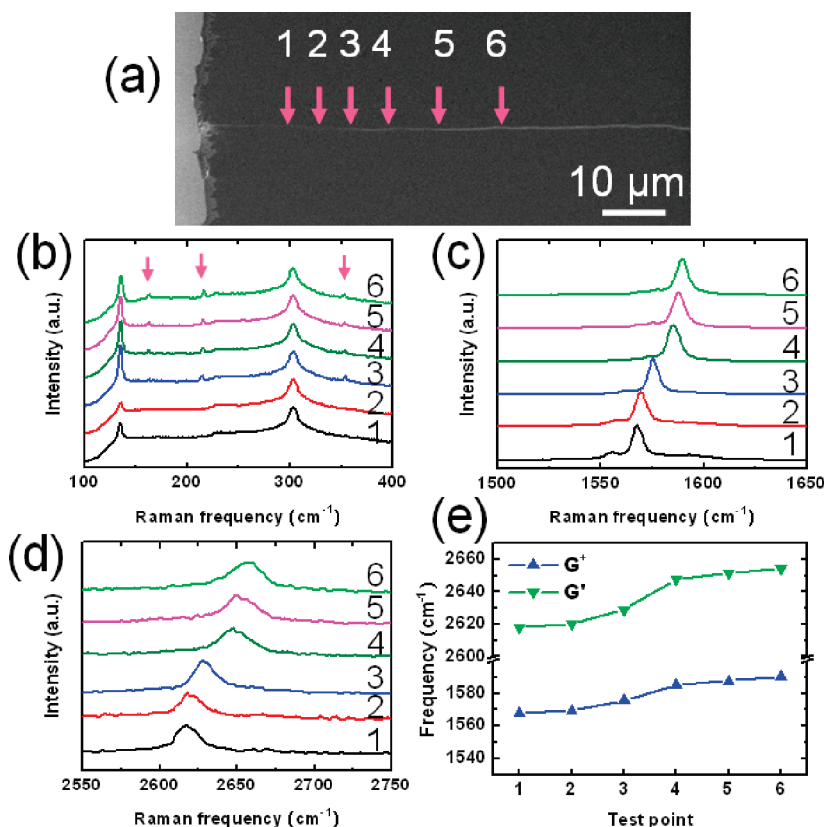

Figure 6. (a) SEM image of another SWCNT. The arrows show different measurement points, i.e., from Point 1 (left) to Point 6 (right), where Raman spectra were collected. (b−d) RBM, G, and G′ Raman modes, respectively. From the bottom to top, the spectra were obtained from the test Points 1−6 in panel a. Note that the Raman spectra show identical features from the Point 6 up to the right end.

is probably caused by the carbon nanodots on/in the SWCNT. The large-diameter SWCNTs are more easily affected by this strain due to the weaker curvature effect, but the branching bundling process can help to prevent the generation of the self-built strain.

EXPERIMENTAL SECTION

The SWCNTs used in this work were synthesized by chemical vapor deposition on Si/SiO$_2$ substrates, with ethanol as the carbon source and Fe particle as the catalyst. The grown tubes are found to be well-separated from each other, and the length extends up to a centimeter. It is found that all SWCNTs grown here have numbers of carbon nanodots on them regardless of their diameters (see Figures 3 and 4a). The resonant micro-Raman spectra were excited using a 632.8 nm (1.96 eV) laser and collected through a 100× air objective. During the entire measurements, we selected a quite lower laser power (<0.2 mW) to avoid any heating effect. The polarization direction of the laser beam was adjusted along with the tube axis. For the laser heating process, the tube was exposed under a 785 nm laser beam (with power of 15 mW) for 10 min.

REFERENCES AND NOTES

1. Minot, E. D.; Yaish, Y.; Sazonova, V.; Park, J. Y.; Brink, M.; McEuen, P. L. Tuning Carbon Nanotube Band Gaps with Strain. *Phys. Rev. Lett.* **2003**, *90*, 156401–156404.
2. Yang, L.; Han, J. Electronic Structure of Deformed Carbon Nanotubes. *Phys. Rev. Lett.* **2000**, *85*, 154–157.
3. Yang, L.; Anantram, M. P.; Han, J.; Lu, J. P. Band-Gap Change of Carbon Nanotubes: Effect of Small Uniaxial and Torsional Strain. *Phys. Rev. B* **1999**, *60*, 13874–13878.
4. Farhat, H.; Son, H.; Samsonidze, Ge. G.; Reich, S.; Dresselhaus, M. S.; Kong, J. Phonon Softening in Individual Metallic Carbon Nanotubes Due to the Kohn Anomaly. *Phys. Rev. Lett.* **2007**, *99*, 145506–145509.
5. Wood, J. R.; Zhao, Q.; Frogley, M. D.; Meurs, E. R.; Prins, A. D.; Peijs, T.; Dunstan, D. J.; Wagner, H. D. Carbon Nanotubes: From Molecular to Macroscopic Sensors. *Phys. Rev. B* **2000**, *62*, 7571–7575.
6. Yuan, S. N.; Zhang, Q.; You, Y. M.; Shen, Z. X.; Shimamoto, D.; Endo, M. Correlation between *In Situ* Raman Scattering and Electrical Conductance for an Individual Double-Walled Carbon Nanotube. *Nano Lett.* **2009**, *9*, 383–387.
7. Huang, Y.; Young, R. J. Non-linear Elasticity in Carbon Fibres. *J. Mater. Sci. Lett.* **1993**, *12*, 92–95.

8. Montes-Morán, M. A.; Young, R. J. Raman Spectroscopy Study of High-Modulus Carbon Fibres: Effect of Plasma-Treatment on the Interfacial Properties of Single-Fibre-Epoxy Composites: Part II: Characterisation of the Fibre-Matrix Interface. *Carbon* **2002**, *40*, 857–875.

9. Souza Filho, A. G.; Kobayashi, N.; Jiang, J.; Gruneis, A.; Saito, R.; Cronin, S. B.; Mendes Filho, J.; Samsonidze, G. G.; Dresselhaus, G.; Dresselhaus, M. S. Strain-Induced Interference Effects on the Resonance Raman Cross Section of Carbon Nanotubes. *Phys. Rev. Lett.* **2005**, *95*, 217403–217406.

10. Cronin, S. B.; Swan, A. K.; Unlu, M. S.; Goldberg, B. B.; Dresselhaus, M. S.; Tinkham, M. Measuring the Uniaxial Strain of Individual Single-Wall Carbon Nanotubes: Resonance Raman Spectra of Atomic-Force-Microscope Modified Single-Wall Nanotubes. *Phys. Rev. Lett.* **2004**, *93*, 167401–167404.

11. Cronin, S. B.; Swan, A. K.; Unlu, M. S.; Goldberg, B. B.; Dresselhaus, M. S.; Tinkham, M. Resonant Raman Spectroscopy of Individual Metallic and Semiconducting Single-Wall Carbon Nanotubes under Uniaxial Strain. *Phys. Rev. B* **2005**, *72*, 035425–035432.

12. Duan, X. J.; Son, H. B.; Gao, B.; Zhang, J.; Wu, T. J.; Samsonidze, G. G.; Dresselhaus, M. S.; Liu, Z. F.; Kong, J. Resonant Raman Spectroscopy of Individual Strained Single-Wall Carbon Nanotubes. *Nano Lett.* **2007**, *7*, 2116–2121.

13. Zheng, L. X.; O'Connell, M. J.; Doorn, S. K.; Liao, X. Z.; Zhao, Y. H.; Akhadov, E. A.; Hoffbauer, M. A.; Roop, B. J.; Jia, Q. X.; Dye, R. C.; Peterson, D. E.; Huang, S. M.; Liu, J.; Zhu, Y. T. Ultralong Single-Wall Carbon Nanotubes. *Nat. Mater.* **2004**, *3*, 673–676.

14. Zheng, L. X.; Satishkumar, B. C.; Gao, P. Q.; Zhang, Q. Kinetics Studies of Ultralong Single-Walled Carbon Nanotubes. *J. Phys. Chem. C* **2009**, *113*, 10896–10900.

15. Jorio, A.; Saito, R.; Hafner, J. H.; Lieber, C. M.; Hunter, M.; McClure, T.; Dresselhaus, G.; Dresselhaus, M. S. Structural (*n*, *m*) Determination of Isolated Single-Wall Carbon Nanotubes by Resonant Raman Scattering. *Phys. Rev. Lett.* **2001**, *86*, 1118–1121.

16. Dresselhaus, M. S.; Dresselhaus, G.; Saito, R.; Jorio, A. Raman Spectroscopy of Carbon Nanotubes. *Phys. Rep.* **2005**, *409*, 47–99.

17. Jorio, A.; Souza Filho, A. G.; Dresselhaus, G.; Dresselhaus, M. S.; Swan, A. K.; Ünlü, M. S.; Goldberg, B. B.; Pimenta, M. A.; Hafner, J. H.; Lieber, C. M.; Saito, R. G-Band Resonant Raman Study of 62 Isolated Single-Wall Carbon Nanotubes. *Phys. Rev. B* **2002**, *65*, 155412–155420.

18. Thomsen, C. Second-Order Raman Spectra of Single and Multiwalled Carbon Nanotubes. *Phys. Rev. B* **2000**, *61*, 4542–4544.

19. Oron-Carl, M.; Hennrich, F.; Kappes, M. M.; Lohneysen, H. v.; Krupke, R. On the Electron-Phonon Coupling of Individual Single-Walled Carbon Nanotubes. *Nano Lett.* **2005**, *5*, 1761–1767.

20. Tsang, J. C.; Freitag, M.; Perebeinos, V.; Liu, J.; Avouris, P. Doping and Phonon Renormalization in Carbon Nanotubes. *Nat. Nanotechnol.* **2007**, *2*, 725–730.

21. Paillet, M.; Poncharal, P.; Zahab, A. Electrostatics of Individual Single-Walled Carbon Nanotubes Investigated by Electrostatic Force Microscopy. *Phys. Rev. Lett.* **2005**, *94*, 186801–186804.

22. Nikitin, T.; Li, X.; Zhang, Z.; Ogasaware, H.; Dai, H.; Nilsson, A. Hydrogen Storage in Carbon Nanotubes through the Formation of Stable C–H Bonds. *Nano Lett.* **2008**, *8*, 162–167.

23. Muniz, A. R.; Singh, T.; Maroudas, D. Effects of Hydrogen Chemisorption on the Structure and Deformation of Single-Walled Carbon Nanotubes. *Appl. Phys. Lett.* **2009**, *94*, 103108–103110.

24. Raravikar, N. R.; Keblinski, P.; Rao, A. M.; Dresselhaus, M. S.; Schadler, L. S.; Ajayan, P. M. Temperature Dependence of Radial Breathing Mode Raman Frequency of Single-Walled Carbon Nanotubes. *Phys. Rev. B* **2002**, *66*, 235424–235432.

25. Grimvall, G. *Thermophysical Properties of Materials*; Elsevier: Amsterdam, 1986.

26. Mohiuddin, T. M. G.; Lombardo, A.; Nair, R. R.; Bonetti, A.; Savini, G.; Jalil, R.; Bonini, N.; Basko, D. M.; Galiotis, C.; Marzari, N.; Novoselov, K. S.; Geim, A. K.; Ferrari, A. C. Uniaxial Strain in Graphene by Raman Spectroscopy: G Peak Splitting, Grüneisen Parameters, and Sample Orientation. *Phys. Rev. B* **2009**, *79*, 205433–205440.

27. Mounet, N.; Marzari, N. First-Principles Determination of the Structural, Vibrational and Thermodynamic Properties of Diamond, Graphite, and Derivatives. *Phys. Rev. B* **2005**, *71*, 205214–205227.